



Mitochondrial Modulation by Dichloroacetate Reduces Toxicity of Aberrant Glial Cells and Gliosis in the SOD1G93A Rat Model of Amyotrophic Lateral Sclerosis

Laura Martínez-Palma^{1,2} · Ernesto Miquel^{1,2} · Valentina Lagos-Rodríguez^{1,2} · Luis Barbeito³ · Adriana Cassina^{2,4} · Patricia Cassina^{1,2}

Published online: 29 August 2018

© The American Society for Experimental NeuroTherapeutics, Inc. 2018

Abstract

Amyotrophic lateral sclerosis (ALS) is a fatal neurodegenerative disease characterized by motor neuron (MN) degeneration and gliosis. Neonatal astrocytes obtained from the SOD1G93A rat model of ALS exhibit mitochondrial dysfunction and neurotoxicity that can be reduced by dichloroacetate (DCA), a metabolic modulator that has been used in humans, and shows beneficial effects on disease outcome in SOD1G93A mice. Aberrant glial cells (AbGC) isolated from the spinal cords of adult paralytic SOD1G93A rats exhibit highly proliferative and neurotoxic properties and may contribute to disease progression. Here we analyze the mitochondrial activity of AbGC and whether metabolic modulation would modify their phenotypic profile. Our studies revealed fragmented mitochondria and lower respiratory control ratio in AbGC compared to neonatal SOD1G93A and nontransgenic rat astrocytes. DCA (5 mM) exposure improved AbGC mitochondrial function, reduced their proliferative rate, and importantly, decreased their toxicity to MNs. Furthermore, oral DCA administration (100 mg/kg, 10 days) to symptomatic SOD1G93A rats reduced MN degeneration, gliosis, and the number of GFAP/S100 β double-labeled hypertrophic glial cells in the spinal cord. DCA treatment of AbGC reduced extracellular lactate levels indicating that the main recognized DCA action, targeting the pyruvate dehydrogenase kinase/pyruvate dehydrogenase complex, may underlie our findings. Our results show that AbGC metabolic phenotype is related to their toxicity to MNs and indicate that its modulation can reduce glial mediated pathology in the spinal cord. Together with previous findings, these results further support glial metabolic modulation as a valid therapeutic strategy in ALS.

Key Words Mitochondria · metabolic modulation · DCA · glial toxicity · aberrant glial cells · ALS

✉ Laura Martínez-Palma
lmartinezpalma07@gmail.com; lmartinezpalma@fmed.edu.uy

✉ Patricia Cassina
pcassina@fmed.edu.uy

¹ Departamento de Histología y Embriología, Facultad de Medicina, Universidad de la República, Av. Gral Flores 2125, 11800 Montevideo, Uruguay

² Centro de Investigaciones Biomédicas (CEINBIO), Facultad de Medicina, Universidad de la República, Av. Gral Flores 2125, 11800 Montevideo, Uruguay

³ Institut Pasteur de Montevideo, Mataojo 2020, 11400 Montevideo, Uruguay

⁴ Departamento de Bioquímica, Facultad de Medicina, Universidad de la República, Av. Gral Flores 2125, 11800 Montevideo, Uruguay

Introduction

Amyotrophic lateral sclerosis (ALS) is a heterogeneous incurable neurodegenerative disease characterized by both upper and lower motor neuron (MN) degenerations leading to severe disability and death within 3 to 5 years of clinical onset. Both sporadic (sALS) and familial (fALS) have similar pathological and clinical features, and diverse genes have been implicated in fALS, sALS, or both [1], leading to the generation of animal models of ALS by expressing mutated genes.

Proposed mechanisms contributing to the disease include defects in multiple key cellular processes in neurons, like excitotoxicity, defective axonal and vesicular transport, changes in RNA metabolism, impaired proteostasis, oxidative

stress, and mitochondrial dysfunction [1]. ALS-associated mitochondrial alterations, including impaired oxidative phosphorylation (OXPHOS) at the electron transport chain (ETC), increased production of reactive nitrogen and oxygen species and defective mitochondrial dynamics, are also directly or indirectly linked to most postulated mechanisms [2]. Furthermore, ALS mitochondrial impairment is not restricted to MN but it is associated with several systemic defects in energy metabolism, including weight loss, hypermetabolism, hyperlipidemia, and glucose intolerance, which correlate with disease outcome [3].

Within the central nervous system, altered mitochondrial function in glial cells may contribute to neurodegeneration. We have previously determined that mitochondria of transgenic (Tg) neonatal astrocytes obtained from the ALS rat model expressing the mutated human superoxide dismutase 1 (SOD1G93A) show a lower oxygen consumption and mitochondrial coupling state compared to mitochondria from astrocytes of nontransgenic (nTg) animals. This metabolic phenotype was associated with a lower capacity to maintain MN survival, which can be prevented by mitochondrial-targeted antioxidants [4]. In addition, improving mitochondrial function with dichloroacetate (DCA) also reduced the proliferation of Tg rat astrocytes, prevented their neurotoxic phenotype, and ameliorated disease progression, spinal MN number, and gliosis in SOD1G93A Tg mice [5].

DCA is a structural analog of pyruvate that has been safely used in humans to treat congenital mitochondrial diseases [6, 7]. It may be orally administered, crosses the blood–brain barrier, and uses the cell monocarboxylate- and mitochondrial pyruvate-transporter system to enter the cells and gain access to mitochondrial matrix, respectively [8]. DCA is the prototypic xenobiotic inhibitor of the pyruvate dehydrogenase kinase (PDK) that regulates glucose metabolism by switching off the mitochondrial pyruvate dehydrogenase complex (PDHC). PDHC is responsible for irreversibly converting pyruvate into acetyl coenzyme A, the primary fuel of the tricarboxylic acid (TCA) cycle, linking glycolysis to OXPHOS [9]. Thus, DCA keeps PDHC in the active, unphosphorylated state, shifting the glycolytic metabolism toward the mitochondria-dependent OXPHOS. This property has recently put DCA in the spotlight in the field of cancer research, as it has been used as a tool to reduce cancer cell proliferation and tumor growth [10].

The role of non-neuronal cells in ALS is currently unquestionable. Neuroinflammation and gliosis are characteristics in the motor cortex and spinal cord from ALS patients and rodent models of inherited ALS. Studies with mutant SOD1 expression in different cell types have led to the concept of ALS as a noncell autonomous disease, highlighting the importance of cell–cell communication between MNs and surrounding glial cells, particularly astrocytes and microglia [11]. Using rodent cell cultures, we and others have provided further evidence in

support of the role of glial cells in MN degeneration, particularly of astrocytes, either reactive [12–14] or SOD1G93A-bearing [15, 16]. Similar results were also obtained with cells derived from fALS and sALS patients [17, 18].

In addition to the pathogenic role of astrocytes and microglia, we have previously described a novel type of aberrant glial cells (AbGC) isolated from the degenerating spinal cord of SOD1G93A rats. AbGC appear after paralysis onset, increase their number toward the final stages of the disease, and are highly toxic to MNs in culture [19]. AbGC simultaneously express astrocytic glial fibrillary acidic protein (GFAP), S100 β , and Connexin-43 (Cx-43) [19] and microglial Iba-1, CD11b, and CD163 markers [20], at least at initial stages of culture. Furthermore, they exhibit features of cellular stress and inflammatory activation [21], a highly proliferative phenotype [19], and induce extensive gliosis after focal transplantation into the spinal cord of nTg rats [22]. Thus, detailed characterization of their toxic phenotype may contribute to understanding pathogenic mechanisms and therapeutic development in ALS.

In this work, we aimed to evaluate AbGC mitochondrial function, its role in the highly proliferative and neurotoxic phenotype of AbGC in culture, and the effects of DCA-mediated metabolic modulation on these parameters as well as on the spinal cord pathology of symptomatic ALS rats.

Material and Methods

Materials

Culture media and serum were from Gibco (Thermo Fisher Scientific, Waltham, MA). Culture flasks and plates were from Nunc (Thermo Fisher Scientific). DCA and all other reagents were from Sigma-Aldrich unless otherwise specified. Antibody data are supplied in Table 1.

Ethics Statement

Procedures using laboratory animals were in accordance with international guidelines and were approved by the Institutional Animal Committee: Comisión Honoraria de Experimentación Animal de la Universidad de la República (CHEA; <https://chea.edu.uy/>); protocol no. 070153-000528-14.

Animals

Rats (*Rattus norvegicus*) were housed (up to 6 female or male animals per cage) in a centralized animal facility with a 12-h light-dark cycle with ad libitum access to food and water.

Male hemizygous NTac:SD-Tg(SOD1G93A)L26H rats, obtained from Taconic (Hudson, NY), were bred locally with outbred Sprague–Dawley background. The progenies were

Table 1 List of antibodies employed for immunocytofluorescence, immunocytochemistry and immunohistochemistry

Antigen	Host, type	Conjugate	Dilution	Vendor, Cat#	RRID
b-III-Tubulin	Rb, P	–	1:3000	Abcam, ab18207	AB_444319
NeuN	Rb, P	–	1:1000	Millipore, ABN78	AB_10807945
Iba1	Rb, P	–	1:1000	Wako, 019-19741	AB_2665520
GFAP	Rb, P	–	1:400	Sigma-Aldrich, G9269	AB_477035
S100 β	Mo, M	–	1:400	Sigma-Aldrich, S2532	AB_477499
Cx-43	Rb, P	–	1:250*	Thermo Fisher Scientific, 71-0700	AB_2533973
GS	Rb, P	–	1:10,000	Abcam, ab49873	AB_880241
GLT-1	Rb, P	–	1:200 [†]	Abcam, ab41621	AB_941782
BrDU	Mo, M	–	1:1000	Sigma-Aldrich, B2531	AB_476793
Rb IgG	Go, P	HRP	1:5000	Thermo Fisher Scientific, 31,460	AB_228341
Rb IgG	Go, P	AF 488	1:1000*	Thermo Fisher Scientific, A-11034	AB_2576217
Mo IgG	Go, P	AF 488	1:1000 [†]	Thermo Fisher Scientific, A-11029	AB_138404
Rb IgG	Go, P	AF 594	1:1000 [‡]	Thermo Fisher Scientific, A-11037	AB_2534095

Cat# = catalog number, RRID = Research Resource Identifier, GFAP = glial fibrillary acidic protein, Cx-43 = Connexin 43, GS = glutamine synthase, GLT-1 = glutamate transporter 1, BrDU = bromodeoxyuridine, Rb = rabbit, Mo = mouse, Go = goat, P = polyclonal, M = monoclonal, HRP = horseradish peroxidase, AF = Alexa Fluor

*1 μ g/ml

[†] 5 μ g/ml

[‡] 10 μ g/ml

genotyped by polymerase chain reaction (PCR), as previously described [15]. Both the onset of symptomatic disease (160–170 days) and lifespan (180–195 days) in our colony were delayed considerably compared with the original report [23].

Primary Cell Cultures

High-glucose (4.5 g/l), pyruvate-free Dulbecco's modified Eagle's medium (DMEM) supplemented with HEPES (3.6 g/l), penicillin (100 IU/ml), streptomycin (100 mg/ml), and 10% (v/v) fetal bovine serum (FBS) (s-DMEM medium) were used for neonatal astrocytes and AbGC cultures. Leibovitz's L-15 medium, supplemented with 0.63 mg/ml bicarbonate, 5 μ g/ml insulin, 0.1 mg/ml conalbumin, 0.1 mM putrescine, 30 nM sodium selenite, 20 nM progesterone, 20 mM glucose, 100 IU/ml penicillin, 100 μ g/ml streptomycin, and 2% horse serum (HS) (s-L15 medium), was used for MN-glial cocultures. Neurobasal medium supplemented with 25 μ M L-glutamate, 25 μ M β -mercaptoethanol, 0.5 mM L-glutamine, B-27 supplement, and 2% HS was used in purified MN cultures (s-NB medium).

Neonatal Rat Spinal Cord Astrocyte Cultures Neonatal rat astrocyte cultures were prepared from Tg SOD1G93A or nTg 1-day-old pups (without regard to sex) genotyped by PCR [14], according to the procedures of Saneto and De Vellis [24] with minor modifications [12]. Briefly, spinal cords were dissected, meninges were carefully removed, and tissue was chopped and dissociated with 0.25% trypsin-EDTA for 25 min at

37 °C. Trypsinization was stopped with s-DMEM medium in the presence of 50 μ g/ml DNase I. After mechanical disaggregation by repeated pipetting, the suspension was passed through an 80- μ m mesh and spun 10 min at 300 \times g. The pellet was resuspended in s-DMEM medium and plated at a density of 1.5×10^6 cells per 25-cm² tissue culture flask. When confluent, cultures were shaken for 48 h at 250 rpm, incubated for another 48 h with 10 μ M cytosine arabinoside, and then plated at a density of 2×10^4 cells/cm² in 4-well plates for cocultures, 25-cm² culture flasks for respirometry studies, or LabTek coverslides chambers for mitochondrial morphology studies.

Aberrant Glial Cell Cultures AbGC were obtained from 6 adult spinal cords of symptomatic SOD1G93A rats (160–165 days; 4 male, 2 female; both hind limbs paralytic) according to the procedures previously described [19]. Briefly, animals were killed by deep anesthesia and the spinal cord was dissected on ice. Meninges were carefully removed, and the rest of the procedure was similar to that described for neonatal astrocyte cultures. Because large amounts of fat hindered cell counting, cells isolated from each individual spinal cord were plated in 1 25-cm² culture flask. Culture medium was removed after 24 h and then replaced every 48 h. Confluence was reached at 3 weeks and AbGC were passaged by trypsinization in the same conditions explained above (at a density of 1×10^6 cells per 25-cm² culture flask) every week. Among passages 4 to 8, confluent AbGC were trypsinized and resuspended in FBS-10% dimethyl sulfoxide (DMSO)

for cryopreservation. For each set of experiments, AbGC from at least 3 rats were used in passages 6 to 12 as previously [19]. For respirometry, mitochondrial morphology, and cocultures, AbGC were plated in the same conditions as neonatal astrocytes.

MN Cultures MN preparations were obtained from embryonic day 15 (E15) nTg rat spinal cords by a combination of optiprep (1:10 in L15 medium) gradient centrifugation and immunopanning with the 192-IgG hybridoma supernatant [25] against p75 neurotrophin receptor as previously described with modifications [4, 12]. Purified MNs were seeded at a density of 300 cells/cm² onto confluent glial feeder layers (FL) in s-L15 medium or on polyornithine-laminin substrate and maintained in s-NB medium supplemented with 1 ng/ml glial cell-derived neurotrophic factor (GDNF) as previously described [12, 19].

Treatment of Cultures and Conditioned Medium Preparation

Stock solution of DCA was prepared in distilled water and directly applied to glial or purified MN cultures at 1:200 dilution and 5 mM final concentration. Treatment of MN was applied 24 h after plating and maintained until survival assessment. AbGC treatment for most experiments was applied on confluent monolayers and chronically maintained for 6 days, replacing medium and DCA every other day, unless otherwise specified. For conditioned medium (CM) preparation, after 6 days of treatment, DCA or vehicle-treated AbGC were washed with PBS and fresh s-L15 medium without treatment was added. CM was collected after 24 h, spun to eliminate detritus and used at a 1:100 concentration [19]. At the same time, fresh s-L15 medium was placed in the incubator to use as control (Ctrl).

Immunofluorescence in Culture

Cells were cultured until confluence; fixed in 4% paraformaldehyde in 0.1 M Dulbecco's phosphate-buffered saline (DPBS) pH = 7.4 for 15 min on ice; permeabilized for 15 min at room temperature with 0.3% Triton X-100 in DPBS; blocked with DPBS containing 10% goat serum, 2% bovine serum albumin (BSA), and 0.3% Triton X-100 for 1 h at room temperature; and incubated overnight in primary antibodies diluted in 0.1% Triton X-100 DPBS. After washing, sections were incubated with the appropriate secondary antibodies conjugated to Alexa Fluor 488 Dye. In some cases, nuclei were stained with 4',6-diamidino-2-phenylindole, dihydrochloride (DAPI, Invitrogen, catalog number D1306). Images were obtained using a digital camera (Olympus DP-71) coupled to an epifluorescence inverted microscope (Olympus IX81) or confocal microscopy (TCS-SP5 II, Leica Microsystems, Wetzlar, Germany).

MN Treatment and Survival Assay

Cocultures were maintained for 48 h and then fixed (4% PFA plus 0.1% glutaraldehyde in PBS, 15 min) and processed for beta-III tubulin immune-peroxidase staining, using a horseradish peroxidase-conjugated goat antimouse secondary antibody and developed with 3,3'-diaminobenzidine. In pure MN cultures, DCA or vehicle-treated AbGC-CM, 5 mM DCA, or s-L15 (control, Ctrl) was added at 1:100 dilution 24 h after plating, and survival was assessed after 48 h. MN survival was evaluated by direct counting of cells displaying neurites longer than 4 cell bodies in diameter, immunoreactive for beta-III tubulin in cocultures, or under phase contrast microscopy in unfixed alive pure MNs using a Nikon Eclipse TE 200 microscope [12, 19].

Mitochondrial Morphology Studies

Confluent glial monolayers seeded on LabTek coverslide chambers were incubated with 100 nM MitoTracker Green FM (Invitrogen, catalog number M7514) for 30 min, washed, and visualized by confocal microscopy (TCS-SP5, Leica Microsystems) using an HCX PL APO × 63/1.40 to 0.60 oil objective. Images were obtained for at least 10 cells per group from 2 experiments, and mitochondrial length was measured manually using the tools (straight or segmented lines length) of Fiji software (NIH; RRID: SCR_002285). At least 280 mitochondria per cell were measured.

Respirometry Studies

After chronic DCA or vehicle treatment, glial monolayers were scraped and resuspended at 2×10^6 cells/ml concentration in culture medium. Then, cell respiration was evaluated using the Oxygraph 2 K respirometer (Oroboros Instruments Corp). Oxygen consumption was recorded at 37 °C in nonpermeabilized intact cells. The rate of oxygen consumption (OCR or O₂ flux) was calculated by the equipment software (DataLab) and was expressed as picomoles of oxygen per milliliter per second.

During recording, basal oxygen consumption (basal OCR) stabilization was followed by sequential addition of 1) the ATP synthase inhibitor oligomycin (oligo, 2 µg/ml), to obtain ATP production related-OCR, 2) successive steps of the uncoupler carbonyl cyanide *p*-trifluoromethoxyphenylhydrazone (FCCP, 0.5 µM each) until maximal respiratory capacity OCR levels was reached, and 3) the mitochondrial complex III inhibitor antimycin A (AA, 2.5 µM) to obtain the nonmitochondrial OCR. AA-inhibited OCR was subtracted from other values to obtain the mitochondrial oligo-inhibited OCR related to ATP synthesis (oligo-inhibited flux–AA-inhibited flux)

and the maximal mitochondrial respiratory capacity OCR (maximum FCCP-uncoupled flux–AA-inhibited flux, MRR). Spare respiratory capacity (SRC) was obtained by subtracting basal OCR from MRR. Mitochondrial function was then expressed as the respiratory control ratio (RCR) index of the intact cells, calculated as the ratio: mitochondrial oligo-inhibited OCR/maximal mitochondrial respiratory capacity OCR. The cell RCR index has the same 2 main advantages as coupling efficiency, which are sensitivity to several potential sites of dysfunction and internal normalization. It is a good marker of mitochondrial dysfunction in cells, as it depends on almost every functional aspect of OXPHOS [26, 27]. Graphical explanation of calculated parameters is shown in the “Results” section (Fig. 2a).

Analysis of Cell Growth and Proliferation

AbGC were plated at a density of 1.2×10^4 cells/cm² in s-DMEM in 35-mm dishes. DCA or vehicle was added 3 h after plating and medium, and DCA was changed every other day. After 1, 2, 3, 6, or 8 days from plating, independent groups of cells were harvested by trypsinization and counted in a Neubauer chamber.

For bromodeoxyuridine (BrdU) incorporation studies, 10 μ M BrdU was added to cultures 48 h after plating, maintained during 6 h and fixed (PFA 4%, 15 min), processed for BrdU immunostaining, and total nuclei were stained with DAPI. Ten images per dish were obtained at $\times 20$ magnification in epifluorescence microscope. DAPI and BrdU stained cells were counted using Fiji software particle analyzer tool and cell counter plug-in respectively. Proliferation was expressed as BrdU immunoreactive cells per 100 nuclei stained with DAPI.

Lactate and Glucose Measurement

AbGC were plated in 35-mm dishes at a density of 2×10^4 cells/cm². DCA or vehicle was added after reaching confluence and medium and DCA was changed at 48 and 96 h. Three 35-mm petri dishes lacking cells were incubated with fresh s-DMEM for 3 days as well as the AbGC. At the 7th day, 72 h AbGC and cell free incubated medium was collected spun and stored at -20 °C until lactate measurement. Lactate and glucose concentration was determined by an automated cell culture analyzer (Bioprofile Basic 2, Nova Biomedical, Waltham, MA). Mean values of measurements obtained from cell-free s-DMEM were subtracted from all data from cell conditioned medium in each experiment. The data are expressed as milligrams per liter corrected per number of cells.

DCA Administration in Animals and Spinal Cord Immunofluorescence

DCA was made fresh at a 500-mg/l concentration in tap water twice a week, and the total consumed volume was measured to ensure a constant daily dose of 100 mg/kg (based on a daily intake of 50 ml) as previously reported for mice [5, 28]. Female rats were used for the experiment. All rats were weighed, and motor activity was observed twice/week from 90 to 100 days of age. Disease onset was determined for each animal when pronounced muscle atrophy was accompanied by abnormal gait, typically expressed as subtle limping or dragging of 1 hind limb. In this moment, animals were randomly assigned to control or DCA treatment group ($n = 5$ per group). Body weight was 286 ± 7.8 in control and 279 ± 10.8 g in DCA group at the start of treatment ($t_8 = 0.538$; $p = 0.606$), and there were no differences after 10 days (276 ± 3.6 in control and 274 ± 11.0 g in DCA group; $t_8 = 0.128$; $p = 0.902$). Five age-matched (± 5 days; body weight 312 ± 11.0 g) control nTg animals were also included. After 10 days of treatment, animals were deeply anesthetized by intraperitoneally ketamine/xylazine overdose (90 and 10 mg/kg respectively) and transcardially perfused with 0.9% saline and 4% PFA in 0.1 M DPBS, pH 7.4. Lumbar spinal cord was removed, postfixed by immersion for 24 h, and then transverse sectioned (30 μ m) in a Leica cryostat. Free-floating immunolabeling was performed. Sections were permeabilized for 30 min (0.3% Triton X-100 in DPBS); blocked with 10% goat serum, 2% BSA, and 0.3% Triton X-100 for 1 h; and incubated overnight or 48 h in primary antibodies for NeuN, Iba1, GFAP, S100 β , or GFAP plus S100 β , diluted in 0.3% Triton X-100 PBS. After washing, sections were incubated in appropriate secondary antibodies conjugated to Alexa Fluor 488 or 594 Dyes. Image stacks and 1 plane images were obtained at $\times 40$ magnification on confocal microscope using the same exposure parameters for all sections.

Image analysis One plane images were examined using Fiji software by an experimenter blinded to treatment. For GFAP and Iba1 immunoreactivity quantification, the ventral horn was delimited in nonprocessed gray scale images from at least 8 nonadjacent sections per animal and mean gray value was measured. Cell counter plug-in was used for cell counting analysis. All double-labeled hypertrophic glial cells present in the ventral horn were counted in merged images from double GFAP/S100 β immunostained sections (at least 10 nonadjacent sections per animal) in which slight brightness/contrast processing was equally applied. MN analysis (cell counting and main diameter measurement) was performed manually with Fiji software basic tools (line perimeter) on single images for at least 15 nonadjacent NeuN immunostained sections per animal.

Presentation of Results and Data

Adobe Photoshop cs6 software (RRID: SCR_014199) was used to process images when indicated and to design figures. GraphPad Prism 5 software (RRID: SCR_015807) was used to design figure graphs and data analysis.

Data from culture experiments are presented as mean \pm SEM of values obtained from at least 3 independently prepared cultures performed in duplicates or triplicates. All data obtained were used for statistical analysis. The significance of differences between 2 sets of data was calculated by the 1-tailed paired *t* test (pairing values within experiments). When comparing more than 2 groups, one-way ANOVA followed by Newman–Keuls multiple comparison test was used. Correlation analysis was performed between means assuming Gaussian distribution of data to obtain Pearson *r* coefficient and r^2 . To compare DCA-treated and untreated time curve of cell growth, two-way ANOVA analysis followed by Bonferroni post-test was performed.

The data from spinal cord assessments are presented as mean \pm SEM of mean values obtained from at least 8 slices per animal, from 5 animals. All data obtained were used for statistical analysis. One-tailed unpaired *t* test was used to compare data from 2 groups and 1-way ANOVA with Newman–Keuls post-test was used for comparing more than 2 groups.

Differences were considered significant when $p < 0.05$; *n*, *F*, and *p* values are provided for each data sets in figure legends.

Results

Aberrant Glial Cells Displayed Lower Mitochondrial Respiratory Function and Length Compared to Neonatal Glia

To analyze mitochondrial function in AbGC, we measured oxygen consumption fluxes by high resolution respirometry (HRR) and compared to nTg and SOD1G93A neonatal astrocytes. HRR of cultured glial cells revealed important differences among the 3 cell types. The cell RCR was lower in neonatal SOD1G93A astrocytes compared to nTg astrocytes as we have previously reported [5]. AbGC exhibited a further reduced cell RCR compared to neonatal Tg astrocytes as shown in Fig. 1a, indicating an even worse mitochondrial functional impairment. Accordingly, mitochondrial morphological features varied among the 3 glial cell types as indicated by MitoTracker Green labeling. As shown in Fig. 1b images, most mitochondria in AbGC were isolated and fragmented compared to the network of filamentous morphology exhibited by nTg astrocytes. Intermediate shapes were found in Tg neonatal astrocytes. The mean mitochondrial length was significantly different among the 3 groups, being highly reduced

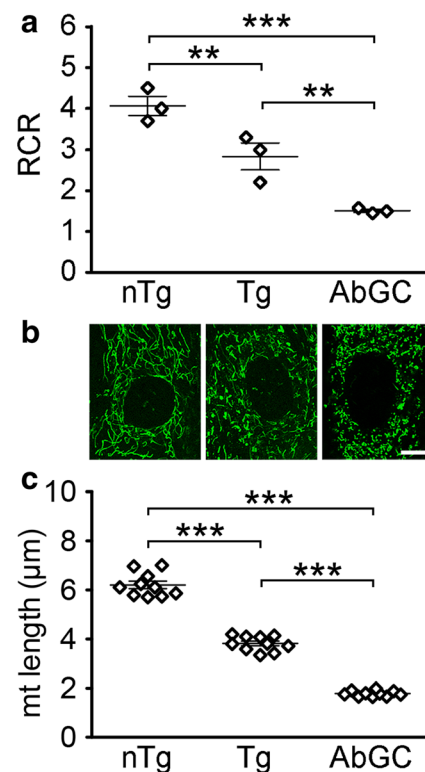


Fig. 1 Reduced mitochondrial function and length in aberrant glial cells compared to neonatal astrocytes. **(a)** Mitochondrial function represented by the cell RCR in neonatal nTg or Tg astrocytes and AbGC after oxygen consumption studies by high-resolution respirometry. Mean \pm SEM from $n = 3$ independent experiments performed in duplicates; $p = 0.0007$; $F_{2,6} = 30.09$; $**p < 0.01$ and $***p < 0.001$. **(b)** Representative confocal microscopy images from MitoTracker Green labeling, scale bar = 10 μm . **(c)** Mean mitochondrial length per cell for the indicated groups. Mean \pm SEM of mean mitochondrial length values from $n = 10$ cells per group (> 280 mitochondria per cell, from 2 independent experiments); $p < 0.0001$; $F_{2,27} = 431.5$; $***p < 0.001$

in AbGC ($1.8 \pm 0.04 \mu\text{m}$) compared to Tg ($3.9 \pm 0.10 \mu\text{m}$) and nTg ($6.2 \pm 0.15 \mu\text{m}$) astrocytes (Fig. 1c). The comparison of the means between cell RCR and mitochondrial length indicates that there is a positive correlation between the 2 variables (Pearson $r = 0.9976$; $r^2 = 0.9951$; $p = 0.0222$).

DCA Improved Mitochondrial Function and Reduced Extracellular Lactate Concentration of Aberrant Glial Cells

To study whether metabolic modulation by DCA could improve the mitochondrial respiration of AbGC, we treated confluent AbGC cultures for 6 days and performed HRR. Figure 2a shows a representative plot of OCR for control and DCA-treated AbGC (upper panel) and a graphical representation of measured mitochondrial parameters (lower panel). The respiratory parameters obtained from the raw data and RCR are shown in Table 2. Basal OCR was not modified by DCA treatment, neither did the ATP production-related respiration. On the other hand, the FCCP-induced MRR was

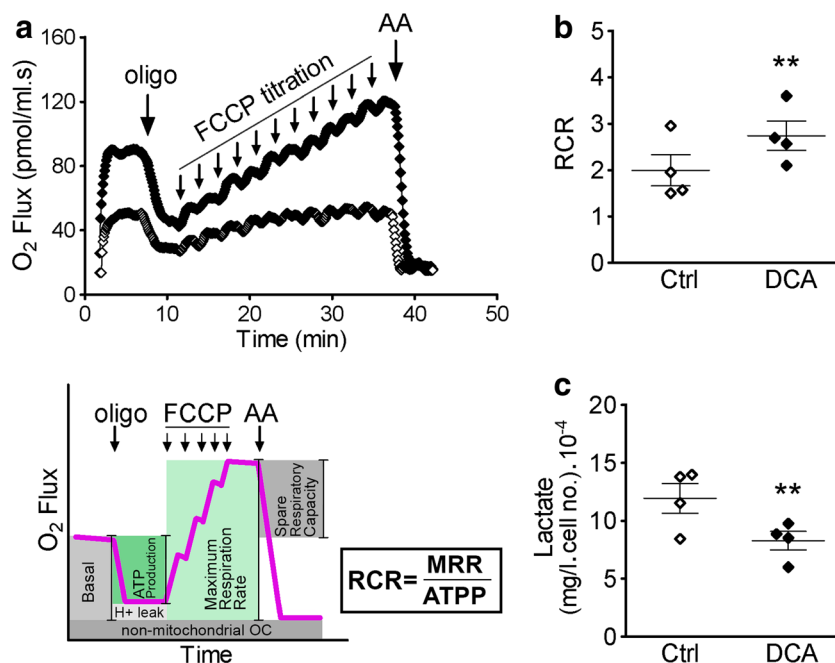


Fig. 2 Increased mitochondrial function and decreased extracellular lactate concentration in aberrant glial cells following DCA treatment. (a) Representative overlapped registers of oxygen consumption rate (O₂ flux) curves from control and DCA-treated AbGC (top) and graphical sketch of respiratory parameters and RCR index (bottom). (b) Cell RCR from DCA chronically treated and control AbGC. Mean ± SEM

from $n = 4$ independent experiments performed in duplicates; $t_3 = 8.311$; $p = 0.0018$; $**p < 0.01$ versus control. (c) Lactate concentration in 3-day conditioned media from chronically DCA treated and control AbGC. Mean ± SEM from $n = 4$ independent experiments performed in triplicates; $t_3 = 5.451$; $p = 0.0061$; $**p < 0.01$ versus control

slightly increased by DCA, as was the SRC. Importantly, the cell RCR for AbGC chronically exposed to DCA was significantly higher compared to nontreated AbGC (Fig. 2b). These results indicate an improvement of mitochondrial functional state and metabolic health induced by the treatment. Furthermore, we found a significant reduction in lactate concentration in the AbGC culture media following chronic treatment with DCA (Fig. 2c). On the other hand, glucose concentration in the culture medium was not modified by the treatment (17.9 ± 3.74 vs $17.4 \pm 3.50 \times 10^{-4}$ mg/l cell number; control vs DCA medium respectively; 2-tailed paired t test; $n = 4$; $p = 0.719$; $t_3 = 0.395$).

DCA Reduced Growth Rate but Did Not Modify the Expression of Typical Phenotypic Markers of Aberrant Glial Cells

When highly proliferative AbGC were exposed to 5 mM DCA from day 0 after plating, cell growth was reduced. DCA exposure significantly decreased the number of cells present in the plates from 2 to 8 days after plating (Fig. 3a). In addition, BrdU incorporation studies performed 2 days after plating showed a reduction of BrdU-stained cells in DCA treatment group (Fig. 3b). However, when applied on confluent cultures,

Table 2 Effects of DCA on respiratory parameters

Parameter	Value ± SEM (pmol/ml s)		p	t	Significance level
	Ctrl	DCA			
Basal	38.5 ± 6.92	44.7 ± 0.67	0.0882	1.761	ns
ATPP	59.4 ± 8.42	73.1 ± 0.63	0.1777	1.090	ns
MRR	47.1 ± 9.51	96.1 ± 4.40	0.0194	3.522	*
SRC	26.7 ± 14.05	41.7 ± 9.42	0.0373	2.686	*
RCR	2.0 ± 0.34	2.74 ± 0.31	0.0018	8.311	†

Basal = basal OCR, ATPP = ATP production-linked OCR (oligomycin inhibited mitochondrial OCR), MRR = maximum respiratory rate (maximum FCCP induced mitochondrial OCR), SRC = spare respiratory capacity (MRC minus basal mitochondrial OCR). $n = 4$, $df = 3$, ns = nonsignificant

* $p < 0.05$

† $p < 0.01$

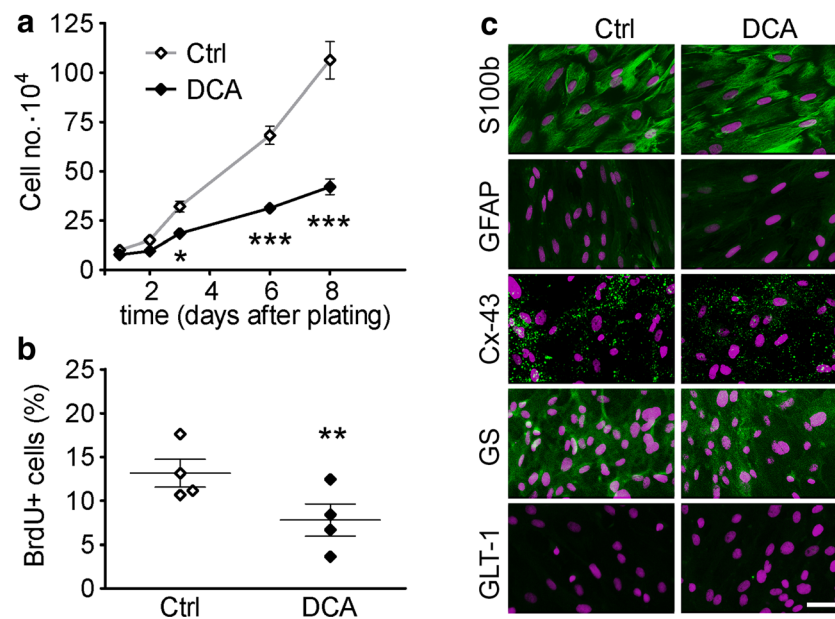


Fig. 3 Reduced aberrant glial cell growth and proliferation without changes in typical phenotypic markers following DCA treatment. (a) Total AbGC numbers counted after harvesting at the indicated times. Mean \pm SEM from three independent experiments performed in duplicates. Two-way ANOVA and Bonferroni posthoc test. For treatment effects, $F_{20,1} = 113.2$; $p < 0.0001$; $*p < 0.05$, $***p < 0.001$ versus control for same time point. (b) BrdU+ cells (% of total

nuclei) after 2 days of DCA or vehicle exposure. Mean \pm SEM from four independent experiments performed in duplicates; $t_3 = 9.320$; $p = 0.0013$; $**p < 0.01$ versus control. (c) Representative images from vehicle (Ctrl, left panels) or DCA (right panels) treated cells immunostained for S100b, GFAP, connexin-43 (Cx-43), glutamine synthase (GS), and the glutamate transporter GLT-1, shown in green. DAPI stained nuclei are shown in magenta. Scale bar = 100 μ m

chronic DCA treatment (5 mM, 5 days) did not modify the number of AbGC, neither attached ($592.0 \pm 11.27 \times 10^3$ control; $604.3 \pm 16.76 \times 10^3$ DCA; 2-tailed paired t test; $n = 3$; $p = 0.664$; $t_2 = 0.504$) nor detached ($9.0 \pm 0.31 \times 10^3$ control; $9.2 \pm 0.50 \times 10^3$ DCA; 2-tailed paired t test; $n = 3$; $p = 0.816$; $t_2 = 0.264$).

On the other hand, chronic DCA treatment did not modify morphological features or expression of previously described AbGC markers analyzed by immunofluorescence. Both vehicle and DCA-treated cells exhibited high immunoreactivity to S100 β , displaying a fibrillary pattern, a low, perinuclear and nonfibrillary GFAP immunostaining, a typical punctate distribution of Cx-43, a moderate cytosolic allocation of glutamine-synthase (GS), and lack of glutamate transporter-1 (GLT-1) immunoreactivity (Fig. 3c).

DCA Reduced Aberrant Glial Cell Toxicity to MNs

To evaluate the effect of DCA on AbGC toxicity to MNs, we assessed MN survival in AbGC-MNs cocultures and in purified MNs exposed to AbGC conditioned medium (CM). As we previously reported [19], CM from AbGC (1:100 dilution) was toxic to purified MN cultures in the presence of GDNF compared to control cultures (upper dashed line), reducing the cell number to the level shown in the trophic factor deprivation condition (lower dashed line) (Fig. 4a). The toxic effect was prevented by chronic DCA treatment of AbGC before CM collection (Fig. 4a). To exclude any direct effect of the

DCA on MN, we treated purified MN with 5 mM DCA in the presence of GDNF for 48 h. Under these conditions, the treatment did not modify MN survival (mean MN number 44.9 ± 2.36 in GDNF-exposed cultures and 45.3 ± 3.38 in GDNF plus DCA exposed cultures; $n = 3$, 2-tailed t test, $p = 0.439$; $t_2 = 0.1713$). In addition, the previously shown highly toxic effect of AbGC to MNs in coculture conditions [19] could also be partially prevented by DCA pretreatment (Fig. 4b). Neuronal survival after 3 days in culture on top of AbGC was very scarce (15% considering 100% the neuronal survival reached on top of neonatal nTg astrocytes feeder layer, upper dashed line). When AbGC were chronically exposed to DCA before MN plating, neuronal survival, albeit still low, was significantly increased (by 62%) compared to untreated ones.

Oral DCA Administration to Symptomatic Rats Reduced Gliosis and MN Loss in the Spinal Cord

We have already shown that DCA treatment improved survival, grip strength, and reduced astrogliosis in SOD1G93A mice [5]. Then, we aimed to investigate whether DCA was also able to modify the previously described pathology in the degenerating spinal cord of the transgenic SOD1G93A rat model of ALS. Oral administration of DCA (500 mg/l in tap water, for a 10-day period) to SOD1G93A Tg rats from symptom onset significantly reduced the already described increment in microglial (Iba1; Fig. 5a, b) and astrocytic (GFAP; Fig. 5c, d) markers in the ventral horn of the spinal cord.

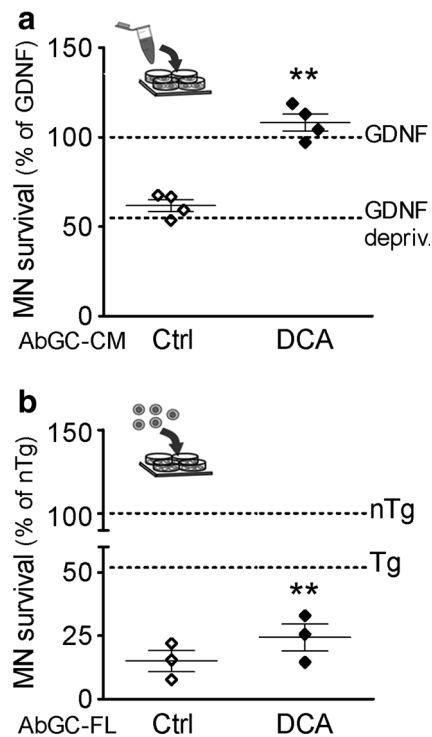


Fig. 4 Reduced aberrant glial cells toxicity to motor neurons induced by DCA. **(a)** Purified MN survival in the presence of GDNF and AbGC CM, expressed as percentage of GDNF-treated CM untreated neurons as control (upper dashed line, 100%); a deprived GDNF control is also shown (lower dashed line). Data are expressed as mean \pm SEM from 4 independent experiments performed in duplicate or triplicate. One-way ANOVA followed by Newman–Keuls multiple comparison test was used to compare the 3 groups; $t_3 = 7.249$; $p = 0.0019$; $**p < 0.01$ versus untreated AbGC-CM and versus GDNF deprivation control. **(b)** Cocultured MN survival on AbGC feeder layer, expressed as percentage of the survival mean on nTg astrocytes in parallel cocultures (upper dashed line, 100%). Survival on SOD1G93A Tg neonatal astrocytes feeder layer is also shown (lower dashed line). MN survival in DCA-pretreated and untreated AbGC cells feeder layer (AbGC-FL) was compared by paired 1-tailed t test. $t_2 = 7.249$; $p = 0.0093$. $**p < 0.01$ versus untreated AbGC-FL

Furthermore, AbGC-like cells (arrows in Fig. 5e), recognized as hypertrophic GFAP/S100 β double labeled cells in the ventral horn of degenerating spinal cords from Tg rats [19], were significantly reduced by DCA treatment (Fig. 5e, f). Most importantly, when we made MN counting and measurements to evaluate MN degeneration, we found that MN number and soma diameter were significantly increased in DCA-treated animals compared to untreated ones (Fig. 5g–i).

Discussion

Here, we show that the high proliferative capacity and toxicity to MNs demonstrated by aberrant glial cells isolated from paralytic rats expressing the ALS-linked SOD1G93A are critically associated to mitochondrial respiratory activity. In fact, when mitochondrial respiration was increased by inhibiting

PDK with DCA, both parameters were reduced. In addition, gliosis and the AbGC-like cell population in the anterior horn of the spinal cord were significantly diminished when DCA was orally administered to early symptomatic rats for 10 days, and more importantly, MN loss and atrophy were also reduced. Remarkably, our findings provide further support that modulation of mitochondrial function may offer benefits to delay paralysis progression in ALS.

Previous morphological studies on AbGC with MitoTracker Green evidenced that mitochondria appear clustered in the perinuclear area and that their main axis was shorter than that observed in neonatal nTg astrocytes as assessed in transmission electron microscopy (TEM) images [21]. Our measurements of mitochondrial length in MitoTracker Green-stained AbGC and nTg neonatal astrocytes were in the range of these previous TEM quantitative data. In addition, we found that astrocytes obtained from SOD1G93A pups had intermediate-sized mitochondria compared to the other 2 groups. These findings suggest that not only the presence of mutated SOD1G93A but also the time of exposure may critically influence mitochondrial size. Mitochondrial morphology and dynamics are known to be associated to respiratory activity, as interconnected mitochondrial networks are frequently present in metabolically and respiratory active cells, whereas small and fragmented mitochondria characterize quiescent and respiratory inactive ones [29]. Indeed, we found a high positive correlation between mitochondrial size and RCR data from HRR assessments in the 3 cell types studied, suggesting differences in their metabolic and redox state [30]. The size and calculated cell RCR for AbGC were the lowest compared to nTg or SOD1G93A neonatal astrocytes. These 2 features, associated to the high proliferation rate [19] and the ultrastructural features [21], revealed high resemblance among AbGC and tumoral cells. Indeed, targeting of AbGC with an antineoplastic drug ameliorated spinal cord pathology, motor outcome, and survival of SOD1G93A rats [31]. Cancer cells are known to exhibit a reduced OXPHOS activity and instead rely on aerobic glycolysis to increase availability of precursors for macromolecule biosynthesis to drive cell growth and proliferation which facilitates cell migration and metastasis [32, 33]. Such phenotype is also characteristic of proinflammatory states of immune cells and glia [34–36]. In this scene, modulating metabolic phenotype appears as an attractive strategy to apply on ALS, in which gliosis and neuroinflammation have been associated to disease progression.

In addition to treating mitochondrial diseases, modulation of mitochondrial function by DCA treatment has been previously applied in cancer cells as a tool to reduce cell growth mainly due to its ability to modify the glycolytic aerobic phenotype by targeting the PDHC/PDK complex [10]. In previous work, we demonstrated that DCA improved mitochondrial respiratory activity and reduced proliferation in cultured rat

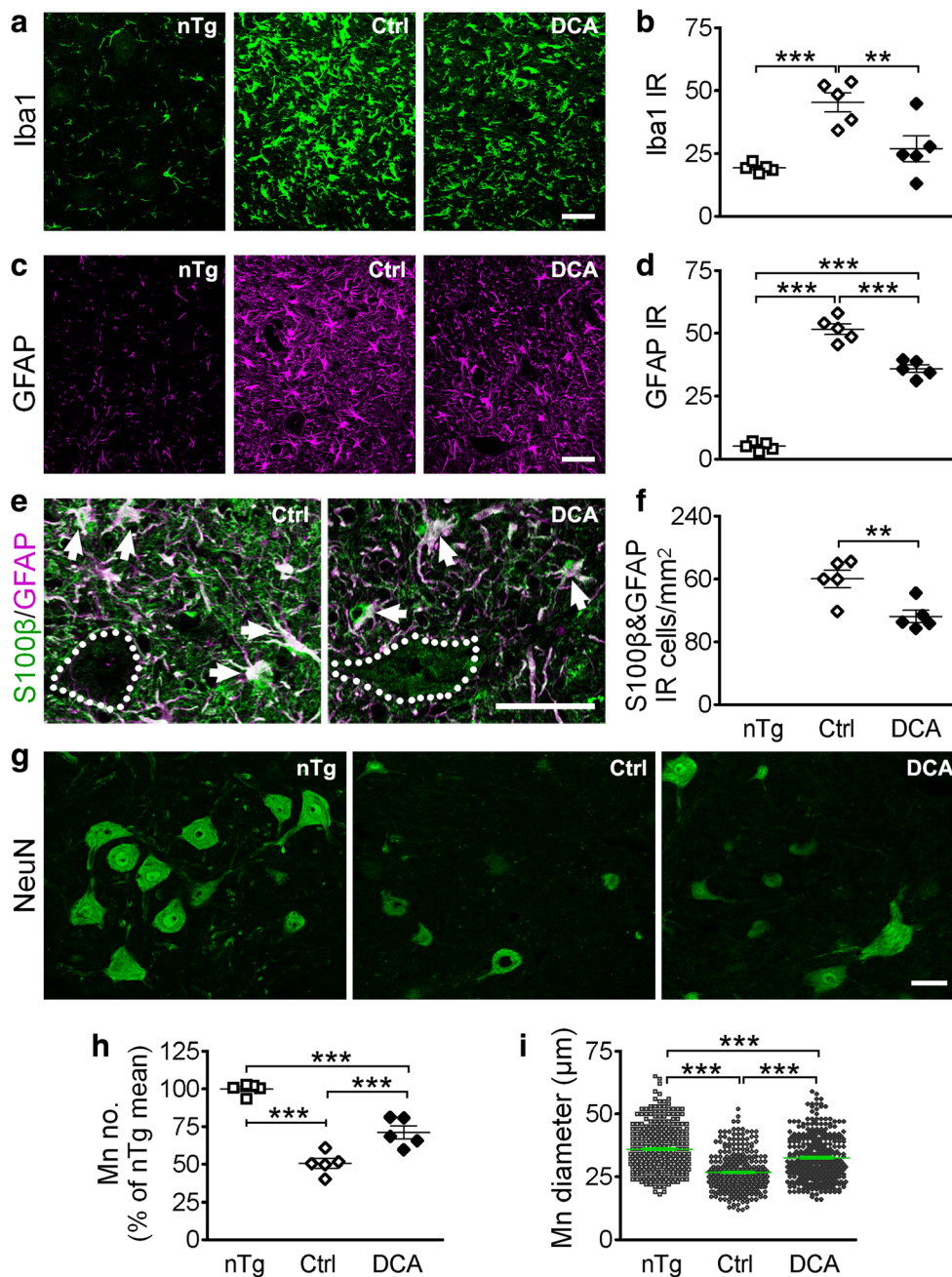


Fig. 5 Reduced gliosis and hypertrophic glial cell number in the spinal cord from symptomatic SOD1G93A rats treated with DCA. Immunofluorescence for cell markers detection was performed in the ventral horn of lumbar spinal cord slices from SOD1G93A rats treated with DCA (500 mg/l in tap water) or vehicle (control) or from age-matched female nTg rats. Quantification data are expressed as mean \pm SEM from $n=5$ animals per group (at least 8 slices per animal). **(a)** Representative Iba1 immunofluorescence images and **(b)** Iba1 immunoreactivity (Iba1 IR) in ventral horn area represented as mean gray density; $p=0.0010$; $F_{2,14}=12.87$; $***p<0.001$ and $**p<0.01$ versus indicated groups. **(c)** Representative images and **(d)** GFAP immunoreactivity (GFAP IR) represented as mean gray density; $p<0.0001$; $F_{2,14}=222.6$; $***p<0.001$ versus other groups.

(e) Immunoreactivity for GFAP (magenta) and S100 β (green); double labeled (white) hypertrophic cells are indicated by arrows; motor neurons are outlined by dashed lines. **(f)** Number of GFAP/S100 β double-labeled cells per square millimeter of ventral horn area; $p=0.0043$; $t_8=3.465$; $**p$ versus Ctrl <0.01 . **(g)** Representative images from NeuN immunofluorescence; MNs were identified by morphological criteria. **(h)** MN number expressed as a percentage of nTg. $p<0.0001$; $F_{2,14}=57.32$; $***p<0.001$ versus other groups. **(i)** Main MN soma diameter of all measured MNs per group; all MNs from each group were pooled, $n=967$; $p<0.0001$; $F_{2,14}=92.54$; $***p<0.001$ versus other groups. Scale bar represents 50 μm in all groups of images

SOD1G93A neonatal astrocytes [5]. Here we show that metabolic modulation also decreases AbGC growth by reducing their highly proliferative profile. However, we did not observe DCA effects on AbGC survival or other phenotypic modifications such as changes in cell morphology, expression, or distribution of AbGC cell markers. DCA actions on cell growth depend on variable molecular mechanisms associated with metabolic state, aging, and/or alterations in mitochondrial ETC [37–39]. In our model, mitochondrial ETC operation seems not to be compromised, as AbGC were capable to enhance cell RCR in response to DCA treatment.

We found a reduction in lactate concentration in the culture media following DCA exposure. Although direct evidence of PDHC phosphorylation was not assayed, this result strongly suggest that the inactivation of PDK leading to a more active dephosphorylation PDHC is the mechanism likely involved in the improvement of mitochondrial respiration in our model. Lactate derived from astrocytes has been considered important to maintain energy metabolism in neurons [40], although quantitative and functional significance is controversial [41], highlighting the importance of compartmental and subcellular concentrations of different metabolites. On the other hand, energy metabolism is altered in brain injury conditions and neurological disorders [40]; indeed, mouse SOD1G93A astrocytes, which have also shown toxic activity to MNs in culture [16, 42], have increased extracellular lactate production compared to nTg astrocytes [42], indicating that a reduced lactate production is not responsible for astrocyte-mediated toxicity. Most importantly, DCA exposure reduced the toxic activity to motor neurons exhibited by SOD1G93A rat astrocytes [5] and also by AbGC as we show here, indicating that the mitochondrial function is critically associated to toxic phenotype of these cells. DCA also lowered AbGC proliferation; however, the reduced toxicity in culture was not due to a decrease in the number of toxic cells but a phenotypic change, as DCA exposure did not modify AbGC number in confluent cultures in which MN survival or CM obtaining was assessed. In our hands, direct exposure of purified motor neurons to DCA, at least to the 5 mM concentration used here, did not modify survival. These results are not unexpected, as previous data showed that neuronal PDHC operates close to maximal activity with low levels of phosphorylated PDH [43]. Thus, inhibition of PDK would target mainly glial cells, particularly those displaying an inflammatory phenotype in which the metabolic profile is more glycolytic, with low levels of active PDHC.

Hypertrophic, GFAP/S100 β double-labeled AbGC-like cells are detected in the spinal cord with the beginning of motor symptoms and increase with the progression of paralysis and MN pathology in the SOD1G93A ALS rat model [19], suggesting a link between the emergence of such cells and disease

spreading. DCA treatment of symptomatic SOD1G93A rats reduced AbGC-like population in the spinal cord, indicating that metabolic changes occur during disease progression. We propose that the metabolic switch detected in aberrant glial cells critically affects neuronal survival in the surrounding area. Astrocytes, being mainly glycolytic, may further augment their glucose utilization by increasing the pentose phosphate pathway and tricarboxylic acid cycle activities under inflammatory conditions [44]. Moreover, the aerobic glycolytic metabolism has been linked to the microglial proinflammatory phenotype [36, 45] which has been associated to a neurotoxic neuroinflammation in ALS [46]. In this sense, taken into account that AbGC share features from both cell types, a metabolic reprogramming induced by DCA would explain the reduction of their neurotoxic properties. Indeed, DCA administration to symptomatic SOD1G93A rats, in addition to diminish hypertrophic AbGC-like cell number, reduced micro and astrogliosis, and partially prevented MN loss and atrophy. These results are in agreement with our previous work, showing reduction of spinal cord pathology, delayed death, and grip strength decline in SOD1G93A mice after DCA treatment [5]. As previously mentioned, the mechanisms involved in DCA effects in our study are likely associated to its actions on glucose metabolism, targeting the PDHC/PDK complex. However, we cannot exclude other actions of the drug such as targeting muscle lipid metabolism, as shown in the SOD1G86R transgenic ALS mouse model, in which DCA treatment also had beneficial effects including delayed symptom onset, improving mitochondrial function, and ameliorating muscle denervation [47] or other effects on systemic metabolism [8].

Although more extensive mechanistic studies are needed, our results provide indirect evidence that support the PDHC/PDK complex as a therapeutic target to delay disease progression in ALS. It would be of great interest to explore these mechanisms in other mouse models of the disease. Although many of the proteins that have been linked to familial and sporadic ALS, including other SOD1 mutations, TDP-43, FUS, and the C9orf72 GGGGCC repeat expansion-associated glycine/arginine (GR) dipeptide repeat protein (DPR), have been shown to induce mitochondrial damage [2], the exact mitochondriopathy has not been fully characterized, and evidence for astrocyte mitochondrial dysfunction associated to MN toxicity has been provided only in the SOD1G93A murine models [5]. DCA has the advantage of having been previously used in human clinical trials to safely treat mitochondrial disorders [6, 7] and brain glioblastoma tumors [48]. Data from cancer research suggest that DCA may have other beneficial properties such as increasing effectiveness and decreasing side effects when used together with standard treatments; indeed,

several DCA derivatives including combined therapies have been proposed [8]. Furthermore, cotargeting independent pathogenic mechanisms would be also beneficial in ALS [49]. Although chronic administration of DCA has been reported to cause peripheral neuropathy, this side effect did not hinder the use of DCA in the treatment of patients and was reversible upon reduction of the dose [6, 48]. In addition, the daily dose of DCA used in our study (100 mg/kg) is much lower than the 1 reported to induce peripheral sensory neuropathy in the rat (500 mg/kg) [50]. The mechanisms underlying these side effects are unknown but may rely on the property of DCA of inhibiting its own metabolism upon repeat dosing, resulting in alteration of its pharmacokinetics. DCA is metabolized to glyoxylate (which is inactive toward PDHC) by glutathione transferase zeta1 (GSTZ1). Genetic variation in GSTZ1 haplotype has been established as 1 of the principal variables influencing DCA kinetics and dynamics in humans apart from previous exposure to DCA [38]. Indeed, personalized dosing of DCA by GSTZ1 genotyping has been recently reported [51].

In conclusion, here we show that metabolic modulation with DCA is effective to decrease AbGC toxicity to MN in culture and to reduce MN loss and gliosis in the degenerating spinal cord of SOD1G93A rats when administered after disease onset. Together with our previous results on the beneficial effects of DCA on ALS mice motor performance and survival, these findings raise the possibility that DCA might have therapeutic benefits in ALS patients.

Acknowledgments: The authors thank Drs. Mariela Bollati and Karen Perelmuter from the Cell Biology Unit at the Institut Pasteur de Montevideo for lactate and glucose measurements. This work was supported by Comisión Sectorial de Investigación Científica (CSIC), Universidad de la República, Uruguay; Grupos I+D Program, #1104 to PC and LB.

Compliance with Ethical Standards

Procedures using laboratory animals were in accordance with international guidelines and were approved by the Institutional Animal Committee: Comisión Honoraria de Experimentación Animal de la Universidad de la República (CHEA; <https://chea.edu.uy/>); protocol no. 070153-000528-14.

Required Author Forms Disclosure forms provided by the authors are available with the online version of this article.

Conflict of Interest The authors declare that they have no conflict of interest.

References

- Brown RH, Al-Chalabi A. Amyotrophic lateral sclerosis. *N Engl J Med* 2017;377:162–172.
- Smith EF, Shaw PJ, De Vos KJ. The role of mitochondria in amyotrophic lateral sclerosis. *Neurosci Lett* 2017. <https://doi.org/10.1016/j.neulet.2017.06.052>.
- Dupuis L, Pradat P-F, Ludolph AC, Loeffler J-P. Energy metabolism in amyotrophic lateral sclerosis. *Lancet Neurol* 2011;10:75–82.
- Cassina P, Cassina A, Pehar M, et al. Mitochondrial dysfunction in SOD1G93A-bearing astrocytes promotes motor neuron degeneration: prevention by mitochondrial-targeted antioxidants. *J Neurosci* 2008;28:4115–4122.
- Miquel E, Cassina A, Martínez-Palma L, et al. Modulation of astrocytic mitochondrial function by dichloroacetate improves survival and motor performance in inherited amyotrophic lateral sclerosis. *PLoS One* 2012;7:1–9.
- Stacpoole PW, Gilbert LR, Neiberger RE, et al. Evaluation of long-term treatment of children with congenital lactic acidosis with dichloroacetate. *Pediatrics* 2008;121:e1223–e1228.
- Abdelmalak M, Lew A, Ramezani R, et al. Long-term safety of dichloroacetate in congenital lactic acidosis. *Mol Genet Metab* 2013;109:139–43.
- James MO, Jahn SC, Zhong G, et al. Therapeutic applications of dichloroacetate and the role of glutathione transferase zeta-1. *Pharmacol Ther* 2017;170:166–180.
- Jha MK, Jeon S, Suk K. Pyruvate dehydrogenase kinases in the nervous system: their principal functions in neuronal-glial metabolic interaction and neuro-metabolic disorders. *Curr Neuropharmacol* 2012;10:393–403.
- Stacpoole PW. Therapeutic targeting of the pyruvate dehydrogenase complex/pyruvate dehydrogenase kinase (PDC/PDK) axis in cancer. *J Natl Cancer Inst* 2017;109:1–14.
- Boillée S, Vande Velde C, Cleveland DW. ALS: a disease of motor neurons and their nonneuronal neighbors. *Neuron* 2006;52:39–59.
- Cassina P, Peluffo H, Pehar M, et al. Peroxynitrite triggers a phenotypic transformation in spinal cord astrocytes that induces motor neuron apoptosis. *J Neurosci Res* 2002;67:21–29.
- Cassina P, Pehar M, Vargas MR, et al. Astrocyte activation by fibroblast growth factor-1 and motor neuron apoptosis: Implications for amyotrophic lateral sclerosis. *J Neurochem* 2005;93:38–46.
- Vargas MR, Pehar M, Cassina P, et al. Fibroblast growth factor-1 induces heme oxygenase-1 via nuclear factor erythroid 2-related factor 2 (Nrf2) in spinal cord astrocytes: consequences for motor neuron survival. *J Biol Chem* 2005;280:25571–25579.
- Vargas MR, Pehar M, Cassina P, Beckman JS, Barbeito L. Increased glutathione biosynthesis by Nrf2 activation in astrocytes prevents p75NTR-dependent motor neuron apoptosis. *J Neurochem* 2006;97:687–696.
- Nagai M, Re DB, Nagata T, et al. Astrocytes expressing ALS-linked mutated SOD1 release factors selectively toxic to motor neurons. *Nat Neurosci* 2007;10:615–622.
- Re DB, Le Verche V, Yu C, et al. Necroptosis drives motor neuron death in models of both sporadic and familial ALS. *Neuron* 2014;81:1001–1008.
- Haidet-Phillips AM, Hester ME, Miranda CJ, et al. Astrocytes from familial and sporadic ALS patients are toxic to motor neurons. *Nat Biotechnol* 2012;29:824–828.
- Díaz-Amarilla P, Olivera-Bravo S, Trias E, et al. Phenotypically aberrant astrocytes that promote motoneuron damage in a model of inherited amyotrophic lateral sclerosis. *Proc Natl Acad Sci* 2011;108:18126–18131.
- Trias E, Díaz-Amarilla P, Olivera-Bravo S, et al. Phenotypic transition of microglia into astrocyte-like cells associated with disease onset in a model of inherited ALS. *Front Cell Neurosci* 2013;7:274.
- Jiménez-Riani M, Díaz-Amarilla P, Isasi E, et al. Ultrastructural features of aberrant glial cells isolated from the spinal cord of paralytic rats expressing the amyotrophic lateral sclerosis-linked SOD1G93A mutation. *Cell Tissue Res* 2017;370:391–401.
- Ibarburu S, Trias E, Lago N, et al. Focal transplantation of aberrant glial cells carrying the SOD1G93A mutation into rat spinal cord induces extensive gliosis. *Neuroimmunomodulation* 2017;24:143–153.

23. Howland DS, Liu J, She Y, et al. Focal loss of the glutamate transporter EAAT2 in a transgenic rat model of SOD1 mutant-mediated amyotrophic lateral sclerosis (ALS). *Proc Natl Acad Sci U S A* 2002;99:1604–1609.
24. Saneto RP, De Vellis J. Neuronal and glial cells: cell culture of the central nervous system. In: Turner A, Brachelard H (eds) *Neurochemistry: a practical approach*. Oxford: IRL Press, 1987, pp. 27–63.
25. Chandler CE, Parsons LM, Hosang M, Shooter EM. A monoclonal antibody modulates the interaction of nerve growth factor with PC12 cells. *J Biol Chem* 1984;259:6882–6889.
26. Brand MD, Nicholls DG. Assessing mitochondrial dysfunction in cells. *Biochem J* 2011;435:297–312.
27. Cassina A, Silveira P, Cantu L, et al. Defective human sperm cells are associated with mitochondrial dysfunction and oxidant production. *Biol Reprod* 2015;93:119.
28. Andreassen OA, Ferrante RJ, Huang H-M, et al. Dichloroacetate exerts therapeutic effects in transgenic mouse models of Huntington's disease. *Ann Neurol* 2001;50:112–116.
29. Galloway CA, Lee H, Yoon Y. Mitochondrial morphology—Emerging role in bioenergetics. *Free Radic Biol Med* 2012;53:1–11.
30. Willems PHGM, Rossignol R, Dieteren CEJ, Murphy MP, Koopman WJH. Redox Homeostasis and Mitochondrial Dynamics. *Cell Metab* 2015;22:207–218.
31. Trias E, Ibarburu S, Barreto-Núñez R, et al. Post-paralysis tyrosine kinase inhibition with masitinib abrogates neuroinflammation and slows disease progression in inherited amyotrophic lateral sclerosis. *J Neuroinflammation* 2016;13:177.
32. Kashatus DF. The regulation of tumor cell physiology by mitochondrial dynamics. *Biochem Biophys Res Commun* 2017;500:9–16.
33. Sun X, Cao H, Zhan L, et al. Mitochondrial fission promotes cell migration by Ca²⁺/CaMKII/ERK/FAK pathway in hepatocellular carcinoma. *Liver Int* 2018. <https://doi.org/10.1111/liv.13660>.
34. Rambold AS, Pearce EL. Mitochondrial dynamics at the interface of immune cell metabolism and function. *Trends Immunol* 2018;39:6–18.
35. Jha MK, Lee IK, Suk K. Metabolic reprogramming by the pyruvate dehydrogenase kinase-lactic acid axis: linking metabolism and diverse neuropathophysiologicals. *Neurosci Biobehav Rev* 2016;68:1–19.
36. Orihuela R, McPherson CA, Harry GJ. Microglial M1/M2 polarization and metabolic states. *Br J Pharmacol* 2016;173:649–665.
37. Delaney LM, Ho N, Morrison J, et al. Dichloroacetate affects proliferation but not survival of human colorectal cancer cells. *Apoptosis* 2015;20:63–74.
38. James MO, Stacpoole PW. Pharmacogenetic considerations with dichloroacetate dosing. *Pharmacogenomics* 2016;17:743–753.
39. Stockwin LH, Yu SX, Borgel S, et al. Sodium dichloroacetate selectively targets cells with defects in the mitochondrial ETC. *Int J Cancer* 2010;127:2510–2519.
40. Barros LF, Brown A, Swanson RA. Glia in brain energy metabolism: a perspective. *Glia* 2018;10–13.
41. Dienel GA. Lack of appropriate stoichiometry: strong evidence against an energetically important astrocyte–neuron lactate shuttle in brain. *J Neurosci Res* 2017;95:2103–2125.
42. Valbuena GN, Tortarolo M, Bendotti C, Cantoni L, Keun HC. Altered metabolic profiles associate with toxicity in SOD1G93A astrocyte–neuron co-cultures. *Sci Rep* 2017;7:1–14.
43. Halim ND, Mcfate T, Mohyeldin A, et al. Phosphorylation status of pyruvate dehydrogenase distinguishes metabolic phenotypes of cultured rat brain astrocytes and neurons. *Glia* 2010;58:1168–1176.
44. Gavillet M, Allaman I, Magistretti PJ. Modulation of astrocytic metabolic phenotype by proinflammatory cytokines. *Glia* 2008;56:975–989.
45. Amici SA, Dong J, Guerau-de-Arellano M. Molecular mechanisms modulating the phenotype of macrophages and microglia. *Front Immunol* 2017;8:1–18.
46. Hooten KG, Beers DR, Zhao W, Appel SH. Protective and toxic neuroinflammation in amyotrophic lateral sclerosis. *Neurotherapeutics* 2015;364–375.
47. Palamiuc L, Schlagowski A, Ngo ST, et al. A metabolic switch toward lipid use in glycolytic muscle is an early pathologic event in a mouse model of amyotrophic lateral sclerosis. *EMBO Mol Med* 2015;7:526–46.
48. Michelakis ED, Sutendra G, Dromparis P, et al. Metabolic modulation of glioblastoma with dichloroacetate. *Sci Transl Med* 2010;2:31ra34.
49. Frakes AE, Braun L, Ferraiuolo L, Guttridge DC, Kaspar BK. Additive amelioration of ALS by co-targeting independent pathogenic mechanisms. *Ann Clin Transl Neurol* 2017;4:76–86.
50. Calcutt NA, Lopez VL, Bautista AD, et al. Peripheral Neuropathy in Rats Exposed to Dichloroacetate. *J Neuropathol Exp Neurol* 2010;68:985–993.
51. Langae T, Wagner R, Horne LP, et al. Personalized dosing of dichloroacetate using GSTZ1 clinical genotyping assay. *Genet Test Mol Biomarkers* 2018;22:266–269.